The unoccupied states of tungsten(001) and tungsten(110): theory and experiment

1991 J. Phys.: Condens. Matter 3 5307

(http://iopscience.iop.org/0953-8984/3/28/006)

J. Phys.: Condens. Matter 3 (1991) 5307–5321. Printed in the UK

The unoccupied states of tungsten(001) and tungsten(110): theory and experiment

I R Collins†, A D Laine†, P T Andrews† and P J Durham‡

† Department of Physics and Interdisciplinary Research Centre in Surface Science, University of Liverpool, PO Box 147, Liverpool L69 3BX, UK
‡ SERC Daresbury Laboratory, Warrington WA4 DA4, UK

Received 5 April 1991

Abstract. The results of relativistic photocurrent calculations, based on the one-step model of photoemission, used here to simulate inverse photoemission spectroscopy (IPES) experiments from the W(001) and W(110) surfaces are presented. The isochromat IPES spectra, for photon energies ranging between 15 and 30 eV, were recorded for electrons incident normal to the (001) and (110) crystal surfaces, corresponding to transitions in the ΓH and ΓN directions of the three-dimensional Brillouin zone, respectively. This combined theoretical and experimental study is used to investigate the electronic structure, in particular the bulk electronic structure, of these systems. The calculated spectra are found to be in good overall agreement with the corresponding experimental results. The origins of the remaining discrepancies between theory and experiment are discussed.

1. Introduction

Angle-resolved photoemission spectroscopy (ARPES) is a well established technique employed to investigate the electronic structure of solids [1]. It has proven to be a unique technique because it can be used to determine the complete set of quantum numbers describing the occupied electron states in the solid, namely energy, momentum, spin and parity. Similarly, momentum-resolved inverse photoemission spectroscopy (KRIPES) has relatively recently been recognized as an important technique for studying the unoccupied electronic states, providing complementary information to that of ARPES [2]. Combining these two techniques therefore provides the possibility of obtaining a complete picture of the solid's electronic structure.

The photoemission process is commonly described by the three-step model [3] in which the process is notionally separated into the adsorption of a photon, the propagation of the photoelectron through the crystal, and its passage through the surface to the detector. In most cases it is possible to compare KRIPES and ARPES data with either bulk band-structure or surface electronic structure calculations, without invoking a rigorous theory for (inverse) photoemission, by simply applying the conservation laws for energy and momentum [4, 2]. The component of the Bloch wavevector $\boldsymbol{k}$ parallel to the surface, $k_{\parallel}$, is conserved in the transition, because the crystal potential parallel to the surface is periodic [5]. However, the component of the Bloch wavevector $\boldsymbol{k}$ perpendicular to the surface, $k_{\perp}$, is not conserved due to the discontinuity at the surface/vacuum interface. Therefore, in the case of IPES performed in the ultraviolet

0953-8984/91/285307+15$03.50

energy region, the problem arises that $k_\perp$ in the final state differs from that of the initial state outside the solid. Some assumption about the electron state inside the solid is often made from that known outside the solid. To a first approximation this assumption usually takes the form of a free-electron-like state accelerated by some energy-independent inner potential [6]. In certain circumstances this approximation can be regarded as justifiable since the initial state ($\sim$ 30 eV above the Fermi level), once smeared out by momentum broadening, could well resemble a free-electron-like band to which the incident electrons may couple [7]. In fact, for solids such as nickel with some initial band matching a free-electron-like band, this approximation appears to be appropriate for KRIPES [8]. However, it is inappropriate for most solids including tungsten, the case in question, where the bands at these energies are far from free-electron-like; see for example the band-structure by Christensen and Feuerbacher [9]. In cases of this nature an accurate description of both the high- and low-energy states in the transition is required to analyse experimental data, i.e. a rigorous theory of (inverse) photoemission needs to be invoked.

In contrast to the three-step model, the photoemission process can be described as a one-step process [10], the matrix element containing the whole of the process, where the bulk and surface electronic structure are treated on an equal footing. This model takes full account of effects such as band-gap photoemission, photoelectron diffraction, multiple scattering, etc [7]. In addition, valuable information, contained within the intensities of the transitions, often disregarded within the three-step model, is provided by this approach. Therefore, the one-step model of photoemission provides a direct and more rigorous comparison with experiment at the one-electron level.

Pendry pointed out that inverse photoemission is time-reversed photoemission [11] and therefore the vast experience of analysing photoemission spectra could be brought to bear on inverse photoemission analysis. In particular, the computational methods which have been developed for calculating photoemission spectra [12] can be applied without modification to inverse photoemission [11]. Over the past decade this non-relativistic one-step theory of (inverse) photoemission has attracted increasing interest, which has been focused on systems where relativistic effects are expected to be negligible, such as in Ni [13–18] and Ag [19, 20]. The availability of a relativistic theory [21–23] enables realistic calculations of (inverse) photoemission spectra of many more systems to be performed. Recently, Ginatempo *et al* [24] have extended the non-relativistic formalism to the fully relativistic limit. These developments can be fully exploited by studying a system where relativistic effects are expected to be strong, i.e. a high-Z system. Here we have used this theory to investigate the electronic structure of tungsten. The effects of relativity, such as band hybridizations, perturbations to band dispersions, lifting of band degeneracies, etc, can be seen in the band-structures of W(001) shown in figure 1 using (a) the non-relativistic limit; and (b) the fully relativistic limit. Aside from these strong relativistic effects which it possesses, tungsten is inherently a very interesting material to study with IPES for various reasons:

(i) the W(001) is found to undergo surface reconstructions [25–27] whose driving force has been linked with the surface electronic structure ([28] and references therein);

(ii) it possesses a large density of unoccupied states, arising from the half-filled d band and is therefore an ideal system to study experimentally [11];

(iii) there are no unoccupied Tamm-like surface states at normal incidence on either the (001) or (110) surfaces [29] permitting a concentrated investigation of the bulk electronic structure, which is of interest here;

(iv) electron correlation effects are not large, so structures such as the satellites seen

on Ni are not expected, permitting the use of density functional theory for interpreting spectra without having to introduce many-body corrections [15];

(v) processes other than IPE, such as the emission of fluorescence photons resulting from the decay of a core hole [30], are not expected to be significant here since the de-excitation of the relatively well bound 4f core holes ($\sim$ 31–33 eV [31]) will be mainly via an Auger process.

Before the advent of KRIPES, k-resolved information about the unoccupied states was provided mainly from secondary electron emission spectroscopy. In fact, Willis and Christensen [32, 33] and Schäfer *et al* [34], using this technique to study tungsten, identified band edges lying above the vacuum zero which were found to be in good agreement with relativistic band-structure calculations [9]. However, recently Drube *et al* [35] measured the unoccupied electronic states of W(001) using IPES. In this study their interest was focused upon the unoccupied surface states since they have been predicted to provide the driving force for the reconstructions of this surface ([28] and references therein). Consequently, the bulk-derived features identified in their spectra were only tentatively assigned to bands in the band-structure and therefore were not analysed in any detail. Similarly Collins *et al* [36], in a following study of the unoccupied surface states of W(001), assigned bulk-derived features identified in their spectra to bands by comparison with a band-structure calculation. In this paper we describe the results of relativistic photocurrent calculations used to interpret normal-incidence IPES spectra from W(001) and W(110); in particular, focusing our attention on the bulk states. These calculations are a valuable tool that produce a complete analysis and therefore a better understanding of the experimental data. In addition, they provide a far more satisfactory comparison between theory and experimental spectra in contrast to adopting a band-mapping procedure.

In section 2 technical details for the calculation of the photocurrents are given and in section 3 the experimental apparatus and procedures are given. The results of the calculations are described in section 4. This section is divided into two subsections, W(001) and W(110) photocurrents, as is section 5, the discussion of these results. The origin of the remaining discrepancies, section 6, is followed by a brief summary in section 7.

2. Calculational details

The photocurrent calculations described here were performed using a recently developed relativistic version of the photoemission code, NEWPOOL, formerly known as PEOVER1 [12]. The formal aspects of the code have been described in detail elsewhere [23, 24] and only its basic principles are briefly outlined here, with specific reference to the inputs used.

Pendry proposed a theory for KRIPES by simply treating the process as time-reversed ARPES, based on the one-step model [11], which had previously been formulated [10, 12]. We shall apply the golden rule expression for ARPES [37, 38] to KRIPES. The photocurrent reaching the detector with a wavevector k, per solid angle and at a given energy, for an electron incident on a solid in state $|j\rangle$ undergoing a transition to an unoccupied state $|i\rangle$ (we use atomic units throughout, with $e = \hbar = m = 1$), is given by

$$J_{\mathrm{ph}}(k) = \frac{\omega^3}{4\pi^2 k c^3} \sum_i |\langle \Psi_j | \delta H | \Psi_i \rangle|^2 \delta(E_j - E_i - \omega) \tag{1}$$

where the sum is over final states i, and δH is the perturbation due to the photon field:

$$\delta H = \frac{1}{2c}(\boldsymbol{A}\cdot\boldsymbol{p} + \boldsymbol{p}\cdot\boldsymbol{A}) \tag{2}$$

$\boldsymbol{p}$ is the momentum operator, and $\boldsymbol{A}$ is the light vector potential with frequency ω. The delta function in equation (1) ensures conservation of energy in the transition.

The two terms in equation (2) can be equated provided a suitable gauge condition is chosen. These terms can then be rewritten using a standard commutator operation [10] as follows:

$$\delta H = \frac{\boldsymbol{A}\cdot\nabla V}{\omega} \tag{3}$$

where V is the potential felt by the electrons.

In the previous description, we limited ourselves to the non-relativistic case. The modifications required for conversion to include relativity, i.e. replacing the Schrödinger equation for the electrons by the corresponding Dirac equation, are non-trivial and have been expounded elsewhere [24].

The golden rule expression can be rewritten in terms of the Green's function for the electrons and is given by

$$J_{\mathrm{ph}} \propto \mathrm{Im}\int \mathrm{d}^3r \int \mathrm{d}^3r'\, \Psi_j^*(r)\,\delta h\, G(r,r';E_j-\omega+\mathrm{i}\epsilon)\,\delta h\,\Psi_j(r') \tag{4}$$

where δh is the normalized perturbation due to the photon field.

This expression is used to evaluate the photocurrent. It is assumed that V has muffin-tin form, a spherically symmetric atomic-like potential at each atomic site, and a flat potential in the interstitial region between the atomic muffin-tins. The electron potential was generated from a self-consistent LMTO-ASA calculation [39]. Using this potential within the relativistic photocurrent code, to calculate a band-structure (a procedure equivalent to a KKR calculation), virtually identical results to those of Christensen and Feuerbacher [9] for energies up to 30 eV above the Fermi level are obtained. The generated band-structure is shown in figure 1. For the photocurrent calculations, this bulk potential is assumed to extend all the way up to the surface. Next it is assumed that the surface is terminated with a one-dimensional step barrier, representing a simplified form of the surface barrier, as depicted in figure 2, whose position and height are treated as input parameters. The height of this barrier was taken to be equal to the Fermi energy above the muffin-tin zero plus the crystal work-function, (4.63 eV [40]). The former two terms are provided by the LMTO-ASA calculation. These approximations are reasonable since, for the purposes of this paper, we are interested in the bulk electronic structure.

With these simplifications, the relativistic photocurrent program works in the following way [12]. The incident electron state Ψ_j, a low-energy electron diffraction (LEED) state, is calculated using a layer-scattering approach in which the solid is divided up into layers of atoms. Ψ_j is expanded in plane waves between the layers, and the reflection and transmission properties of each layer are calculated, giving the probability amplitudes for a plane wave with parallel wavevector component $k_\parallel$ to be reflected and transmitted into plane waves $k_\parallel + G_\parallel$. By repeated reflection and transmission operations, the full wavefunction of the electron incident on the whole

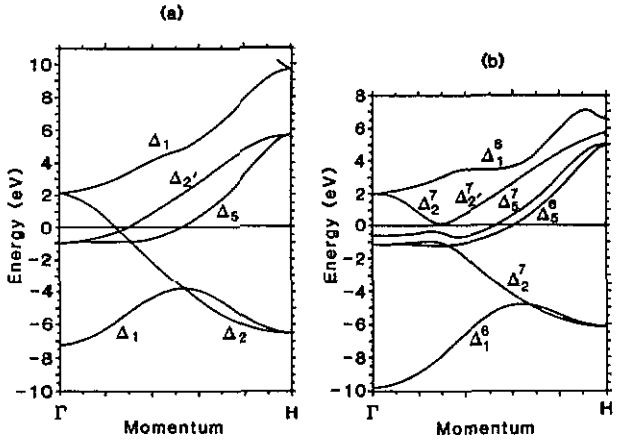

Figure 1. Band-structure of tungsten along the [001] axis, the ΓH direction, for (*a*) non-relativistic calculation and (*b*) fully relativistic calculation. Symmetry labels are subscripted with single group representations to which the bands would belong in the absence of spin–orbit coupling and superscripted with the double group representations.

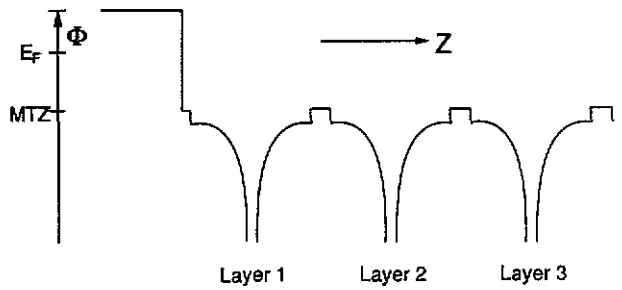

Figure 2. Schematic diagram of the idealized solid. The bulk one-electron muffin-tin potential, assumed here to extend up to the surface, is terminated by a one-dimensional step barrier representing a simplified form of the surface barrier.

semi-infinite crystal can be determined. Knowing Ψ_j and with the simplification that δh (i.e. grad V) is only non-zero inside the muffin-tins and at the surface potential step, it is then straightforward to use the layer-adapted multiple-scattering technique to calculate the whole wavefield.

The highest l value for the spherical wave expansion is 4 and the number of layers is restricted to 128 for final state energies and 16 for initial state energies. Twenty-five beams in the plane wave representation of the LEED states were found sufficient to achieve convergence of the photocurrent.

Imaginary parts of the potential are included, assumed here to be energy-independent, at both the high-energy (Ψ_j) and the low-energy (Ψ_i) states thereby simulating mean-free path and lifetime broadening effects, respectively. For the former, an inverse lifetime of −0.1 Hartrees (−2.72 eV) was used in accord with typical electron escape depth data from tungsten at energies of about 30 eV [41]. An inverse lifetime of −0.002 Hartrees (−0.05 eV) was taken, for the broadening of the low-energy state (final state), from lifetime measurements of the $N_{6,7}$ Auger transition [42].

The quantity calculated by the program, equation (4), is the probability of an

electron, incident in a particular direction defined by the angles θ_e, ϕ_e, undergoing a transition between two unoccupied states emitting a photon of energy ω, in a particular direction defined by the angles θ_p, ϕ_p, with a particular polarization. The geometrical arrangement of the various directions are depicted in figure 3. These parameters were defined in order to simulate the experimental conditions, see section 3. Here the polarization of light was defined to be either s or p polarized (with the electric vector $\boldsymbol{E}$ out of(in) the plane of electron incidence and emitted light, respectively), and, since the polarization of light is not measurable in our experiments, the two resulting spectra are simply added to give a total unpolarized photocurrent. Although this program has the facility to calculate spin-polarized spectra, these photocurrent calculations were made taking the non-spin-polarized limit since a non-spin-polarized electron source was used in our experiments described in section 3.

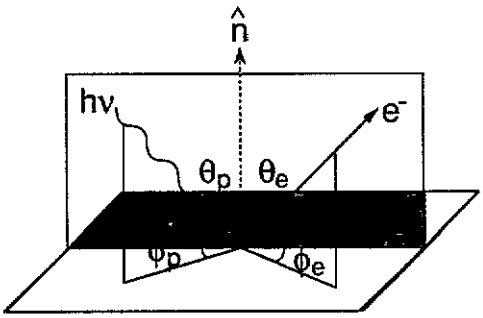

Figure 3. Geometrical arrangement defining the angles and directions of the electron and photon in the photocurrent calculations.

At present, photocurrents can be computed for the fairly close-packed systems, such as the (001) and (110) surfaces of cubic crystals. However, problems arise for the more open structures, such as the (111) surfaces, where the lattice planes parallel to the surface are very close together, and the expansions for the wavefunctions in the interstitial region between the planes may not converge.

The running time of the code was less than 10 s/point, calculated using the CRAY-XMP computer at the Rutherford Appleton Laboratory, UK.

3. Experimental details

The IPE apparatus and experimental procedures have been described in detail elsewhere [36]. All the measurements were made in the isochromat mode by scanning the incident electron energy and measuring the photon flux for a fixed photon energy. For the experiments described in this paper the electrons were incident normal to the crystal surface with a grating monochromator selecting photon energies between 15 and 30 eV, so scanning different regions of $E, k_\perp$ space. The locations of the electron gun and the grating within the chamber are fixed, subtending an angle of 40° at the specimen. The 92 mm diameter grating mounted on the Rowland circle of diameter 300 mm collects light over a solid angle of 0.024π sr. The azimuthal orientation of the crystals was defined such that the emitted light was collected in the [100] mirror plane, $\bar{\Gamma}\bar{X}$ direction, for the (001) surface and in the $[1\bar{1}0]$ mirror plane, $\bar{\Gamma}\bar{N}$ direction, for the (110) surface.

The total energy resolution as a function of photon energy was determined empirically from the observed Fermi level threshold of polycrystalline gold, the results of which are shown in figure 4. All the experiments were performed in a vacuum of better than 8×10^{-11} mbar and data were recorded at or above room temperature after flashing the crystal to a temperature of $\sim 2500\,^{\circ}\mathrm{C}$ in order to restore the clean surface. Spectra were recorded for up to 1.5 h at the spectrometer base pressure before recleaning, this procedure being repeated until satisfactory statistics had been accumulated.

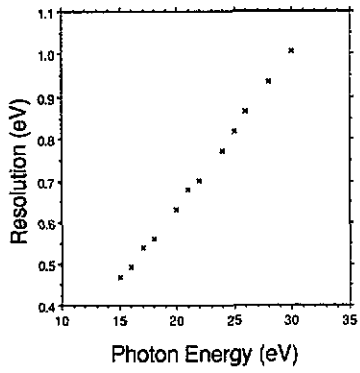

Figure 4. Plot showing the experimental energy resolution, FWHM (eV), as a function of photon energy, as determined from the observed Fermi level threshold of polycrystalline gold.

4. Photocurrent calculations

The relativistic photocurrent calculations were computed for electrons incident normal to the W(001) and W(110) surfaces, $k_{\parallel} = 0$, with the light emitted at 40° from the surface normal in the [100] and [1$\bar{1}$0] mirror planes respectively, for a series of photon energies. The position of the surface step barrier was chosen to position a strong surface-related feature below the Fermi level, since no surface-related feature is observed above the Fermi level at $k_{\parallel} = 0$ on the W(001) surface [36] (Drube *et al* [35] observed a surface resonance at $k_{\parallel} = 0$ near Γ). This surface-related feature most probably corresponds to the well-known 'Swanson hump state' [43] located at Γ, 0.3 eV below E_F ([44] and references therein).

Symmetry labels, shown in figures 1 and 5, are subscripted with single group representations, to which the bands would belong in the absence of spin–orbit coupling and superscripted with the double group representations.

4.1. W(001)

The bulk band-structures of W(001), corresponding to the ΓH direction, are shown in figure 1, thus indicating the possible final state bands to which the incident electron may couple.

In figure 6 the calculated spectra, for all photon energies, exhibit well defined structures superimposed upon a broad distribution of intensity. Here we can use symmetry

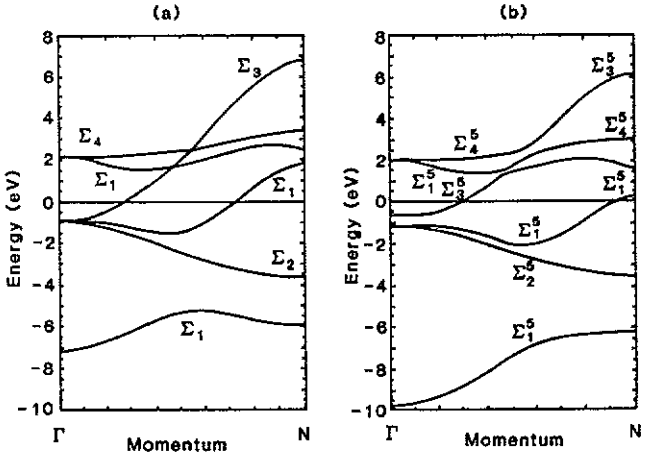

Figure 5. Band-structure of tungsten along the [110] axis, the ΓN direction, for (*a*) non-relativistic calculation and (*b*) fully relativistic calculation. Symmetry labelling as defined in figure 1.

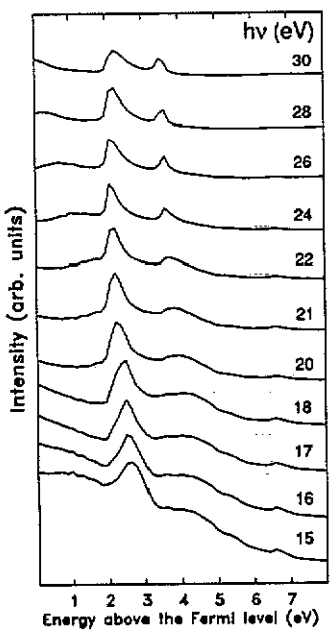

Figure 6. Calculated normal-incidence isochromat IPE spectra from W(001) for various photon energies.

arguments to identify the origin of the final states involved in the direct interband transitions. Transitions to the Δ_2 and $\Delta_{2'}$ bands, in the non-relativistic limit (figure 1) are forbidden for normal incidence electrons [45]. This selection rule does not strictly hold in the relativistic limit [46], due to the spin–orbit coupling allowing the $\Delta_1, \Delta_2, \Delta_{2'}$ and Δ_5 bands to hybridize, as can be seen in figure 1. However, one would not expect any significant photocurrent contribution to arise from the $\Delta^7_{2,2'}$ band since

it is mostly derived from the Δ_2 and $\Delta_{2'}$ bands with a small admixture of the Δ_5 band. This implies that the intensity between the Fermi level and 2 eV, where the unoccupied Δ_1^6 band begins, must therefore arise from transitions to the $\Delta_5^{6,7}$ band over a wide range of momenta. The dominant features in these spectra are the peaks varying between 2.1 and 2.6 eV, and between 3.5 and $\sim$ 4.3 eV. By inspection of the bulk band-structure both these features are attributed to transitions into the Δ_1^6 band. The former resulting from transitions in the first third of the ΓH line in the low photon energy spectra and moving towards Γ in the high photon energy spectra. The latter dominant feature resulting from transitions into the plateau region of the Δ_1^6 band in the high photon energy spectra. This feature appears to broaden as the photon energy is reduced from the 22 eV spectrum to the 15 eV spectrum probably indicating an additional contribution to this peak from the rapidly dispersing $\Delta_5^{6,7}$ band near the H point. The weak peak at 6.6 eV, which is independent of photon energy and whose intensity is more pronounced for the low photon energy spectra, is due to a high density-of-states of the Δ_1^6 band at the H point.

4.2. W(110)

The bulk band-structures of W(110), corresponding to the ΓN direction, are shown in figure 5.

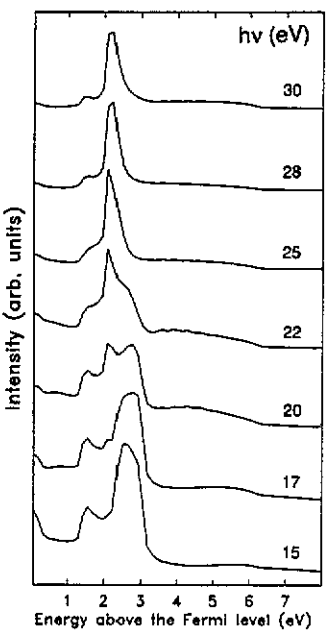

Figure 7. Calculated normal-incidence isochromat IPE spectra from W(110) for various photon energies.

The situation with the W(110) photocurrent calculations, shown in figure 7, is similar to that of W(001), although here all the accessible final states are symmetry-allowed at normal incidence in the non-relativistic limit [45], and hence in the relativistic limit. The intensity between the Fermi level and 1.5 eV, where the flat Σ_1^5 and Σ_4^5 bands begin, arises from transitions into the Σ_3^5 band since this is the only

final state band between 0.3 and 1.5 eV above the Fermi level. However, the intensity observed at the Fermi level in the low photon energy spectra probably arises from transitions into the Σ_1^5 band, appearing just above the Fermi level near the N point. The dominant structure in the spectra is a series of peaks between 1.5 and 2.8 eV. On increasing the photon energy from 15 eV, where two peaks are observed at 1.5 and 2.8 eV, to the 30 eV spectrum, where mainly a single peak at 2.1 eV is observed, considerable changes in the lineshape occur. In this case, it is difficult to accurately identify the origin of these peaks because there are a number of flat bands in this direction at this energy, see figure 5. The broad shoulder at ~ 6 eV, which is photon energy independent, is attributed to a high density-of-states of the Σ_3^5 band at the N point.

It should be noted here that the intensity of the dominant features in the calculated spectra relative to the broad background distribution is more pronounced in this case than in that of W(001). This presumably arises from the relatively flat final states with a concomitant high one-dimensional density-of-states in this direction.

5. Discussion

Before we examine the agreement between these calculations and experimental data, the computed spectra require broadening with the experimental resolution function, assumed to be Gaussian-like, whose width (FWHM) as a function of photon energy is given in figure 4.

5.1. W(001)

In figure 8 the photocurrent calculations are shown alongside isochromat IPES spectra taken at the corresponding photon energies. The overall intensity distribution of the predicted spectra are in good agreement with experiment with most of the intensity originating from transitions into states between 2 and 5 eV above E_F. Experimentally, the intensity at the Fermi level relative to the spectrum maximum increases with increasing photon energy, reaching a maximum in the 18 eV spectrum, thereafter diminishing with photon energy. At the highest photon energies recorded this intensity again increases. This trend in intensity at the Fermi level is accurately reproduced in the calculations.

Structures in the calculations, such as the peak at ~ 2.6 eV, can be clearly identified with those in the data; however, the state in question is observed at ~ 3 eV. The peaks predicted to disperse from ~ 4.3 to 3.5 eV for increasing photon energies correspond well with the observed structure between ~ 4 and 5 eV, although only observed in the higher photon energy spectra. It should be noted here that the calculated spectra appear to be shifted to lower energies by about 0.5 eV. This shift may be due to a number of contributions, such as:

(i) errors in the momentum of the initial state, which lead to errors in the energy of the direct transitions especially when $\delta E/\delta k$ is large, as it is for the Δ_1^6 band contributing to these features;

(ii) self-energy shifts;

(iii) inaccuracies in the bulk potential in the surface region; and

(iv) deficiencies in the calculation. These contributions will be discussed in some detail in section 6.

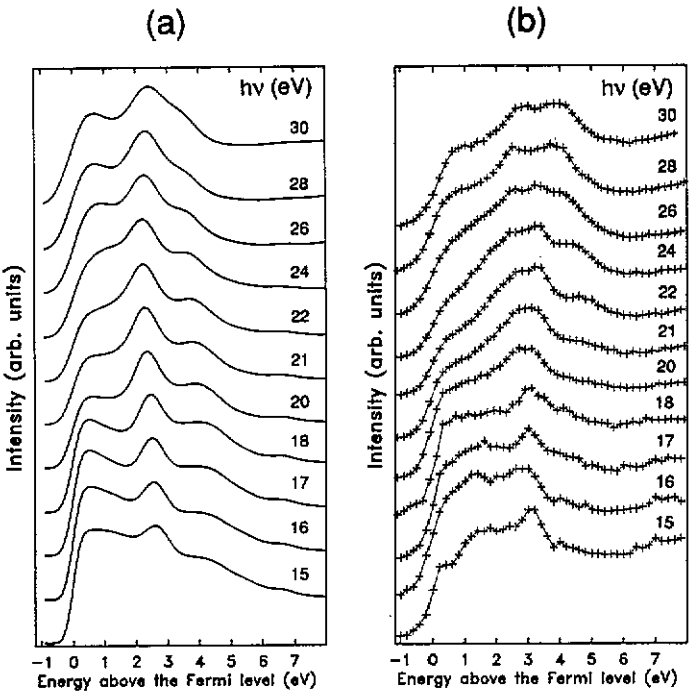

Figure 8. Comparison of (*a*) the photocurrent calculations convoluted with the experimental resolution function, full curves, and (*b*) experimental IPE spectra, crosses, for the W(001) surface.

5.2. W(110)

In figure 9 the photocurrent calculations are shown superimposed on isochromat IPES spectra taken at the corresponding photon energies. The excellent agreement between theory and experiment can immediately be seen. Not only are the energies and intensities of the states reproduced but also their changes as a function of photon energy. For example, the intensity close to the Fermi level relative to the peak around 2–3 eV is accurately predicted. The small discrepancies in peak energies are possibly a result of effects (ii), (iii) and (iv) described in section 5.1. A consistent underestimate in the predicted peak widths is apparent in the spectra shown in figure 9 possible arising from either the effect of assuming energy-independent lifetimes or self-energy effects. These contributions are described in detail in the following section.

6. Origin of discrepancies

The effects leading to the discrepancies between theory and experiment, outlined in the previous section, require further discussion.

Self-energy effects arise from the fact that density-functional theory [47] predicts the ground state properties of an interacting many-electron system, whereas, experiments measure the system in an excited state, for example, IPES probes the $(N + 1)$ electron system. The self-energy, whose real part gives an energy shift and whose imaginary part gives a lifetime broadening to the quasi-particle energy bands, behaves like a complex, energy-dependent potential and could in principle be added to

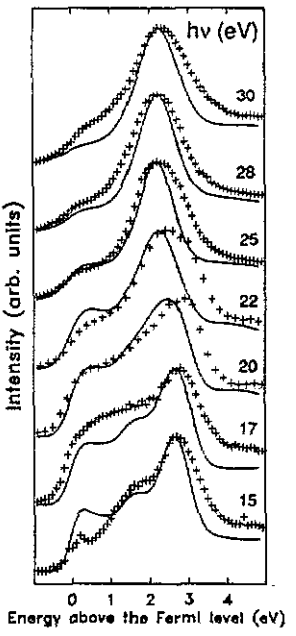

Figure 9. A direct comparison, by superposition, of the photocurrent calculations convoluted with the experimental resolution function, full curves, and the experimental IPE spectra, crosses, for the W(110) surface.

V, the potential, in the calculation. Self-energy effects, expected to increase with energy above E_F, should exist. In fact, Speier *et al* by comparing bremsstrahlung-isochromat spectroscopy measurements and density-of-states calculations for metals, such as Ag and Pd, found discrepancies between energy positions in the experimental and theoretical structures, which were small below 10 eV above E_F, and were of the order 1–2 eV at $\sim$ 20 eV above E_F [48]. These results would suggest that, due to self-energy effects, our calculated final and initial states could be shifted by similar magnitudes, respectively. These contributions at both energies could affect the energies of the predicted final states. The W(110) results, where the final state bands are relatively flat, suggest that the self-energy correction in the final state is indeed small since excellent agreement is found between the predicted and observed final state energy positions. However, the self-energy correction is more serious in the initial state. In particular, for rapidly dispersing final state bands, such as in the W(001) case, a discrepancy in the momentum of the initial state could produce a discrepancy in the predicted energy position of the final state. Furthermore, a possible explanation for the observation of the consistently underestimated linewidth of the predicted peaks may also lie in the neglect of self-energy effects. We suggest here that self-energy effects are perhaps not the dominant contribution for these discrepancies between theory and experiment. In this study it is perhaps premature to attribute these discrepancies to self-energy corrections before other effects are quantified. In doing so, one can in principle determine to what extent self-energy corrections are important.

The neglect of treating the surface in a realistic manner can sometimes lead to errors in the description of the surface density-of-states and might also introduce slight inaccuracies of the bulk potential in the surface region. Recently König *et al* [19] showed that, in the case of Ag(001), inclusion of realistic potentials at the sur-

face and an improved treatment of the surface barrier, both generated from a separate scalar-relativistic full-potential linearized augmented-plane-wave thin-film calculation, produced energy shifts in the bulk-derived features as large as 0.3 eV compared with those assuming a single bulk potential and a step-like surface barrier. The importance of this contribution is reflected in the magnitude of the surface core level shifts (SCLS). The SCLS are a consequence of the reduced coordination of atoms at the surface. In order to retain charge neutrality the potentials in the surface region shift in energy relative to that of the bulk [49, 50]. The SCLS of tungsten have been studied extensively [51], the results showing shifts of −0.36 eV (surface) and −0.14 eV (sub-surface) for W(001) [52] and −0.321 eV (surface) for W(110) [31]. Of course this surface effect will only be significant for electrons penetrating a short distance into the solid, say probing only the top few layers. Indeed, a layer-by-layer decomposition of a calculated bulk state reveals intensity arising predominantly from the top few layers. This effect is expected to be more pronounced for the (001) surface compared with the (110) surface since the inaccuracy of our description of the potential in the surface region extends further into the crystal; the W(110) spectrum has only one surface-shifted component [31]. The clean surface of W(001) is found to reconstruct [25–27]. In the calculations presented here, no attempt has been made to model a reconstruction of the W(001) surface since, for the purposes of this paper, we are mainly interested in the bulk properties of these systems, and therefore the simplification of neglecting such surface effects is perhaps appropriate. Moreover, LEED measurements taken on our W(001) crystal show a sharp (1 × 1) pattern, consistent with the observation of previous workers [27], thus confirming that this surface was unreconstructed.

The use of a step-like barrier at the surface does not predict the existence of image potential states, arising from the electron outside the surface being trapped by its own image potential, since image potential states are derived from the long-range nature of the surface barrier [2]. Consequently, only the use of an asymptotic-like surface barrier will predict the existence and the energies of the image states. In fact, a possible image state is observed experimentally at normal incidence on the W(001) surface at 4 eV above E_F. This state is tentatively observed in the lowest photon energy spectra but is completely masked by the prominent feature seen at $\sim$ 3 eV in the higher photon energy spectra. However Drube *et al*, using IPES employing different experimental conditions, clearly observed an image potential state on the W(001) surface at 3.9 eV above E_F [35].

A possible deficiency in the calculations is the simplification of energy-independent imaginary parts of the effective potential at both the initial and final state energies. McRae [53] showed that the energy dependence of the imaginary part of the effective potential increases linearly between 1 and 4 eV for electron energies ranging between 10 and 50 eV. Our calculated photocurrent was found to be fairly insensitive to variations of this energy-independent parameter in the initial state, as one would expect for a bulk terminated surface since it simply determines a mean free path of the incident electron, and therefore the simplification made here is perhaps justified. The lifetime broadening in the final state, i.e. between E_F and a few electron volts above, is not expected to exhibit such a large variation and therefore our simplification is more appropriate. The underestimate of the linewidth in the predicted spectra shown in figure 9 could be completely reflected in the choice of this parameter, which was determined from experimental data, see section 2. However, recent ARPES results from W(110) suggest that the energy and momentum linewidths of the observed states are anomalously broadened compared with the predictions of theories based purely upon

lifetime broadening of the final-state photohole and photoelectron [54]. These observations were interpreted in terms of the excitation of phonons during the photoemission process.

The photocurrent calculations do not include processes such as electron–hole creation [55] or the emission of fluorescence photons caused by the decay of a core hole [30], which are known to contribute to background intensity in the IPES spectrum. The neglect of the former effect is less serious in the case of W(110) where the intensity into the d bands relative to the background intensity is large, presumably due to the relatively flat bands with a concomitant high one-dimensional density of states, compared with that of W(001), see figures 8 and 9. The latter effect, in the case of tungsten, can only contribute intensity for electron energies greater than ~ 31 eV (the binding energy of the 4f electrons, ϵ_{4f}) and photon energies greater than ~ 24 eV (ϵ_{4f}-valence band width). This effect is not expected to be significant here since the 4f core holes will decay mainly via an Auger process and not via the emission of fluorescence photons.

A more serious problem is the simplification of a constant photon field, with no refraction, screening, and the same fields inside as outside the crystal. It would be difficult to improve on this assumption since the surface dielectric response of metal and semiconductors is not known with any accuracy, depending in a complicated way on the wavefunctions [56].

7. Conclusions

We have performed relativistic photocurrent calculations, based on the one-step model of photoemission, simulating normal-incidence isochromat IPES spectra from W(001) and W(110), where relativistic effects are expected to be large, in order to investigate their bulk electronic structure. The calculated spectra are found to be in good overall agreement with the corresponding experimental results, thereby confirming the validity of the theoretical approach. The remaining discrepancies between theory and experiment are assigned to inaccuracies in the description of the surface, both in the potentials and in the description of the surface barrier, and to deficiencies in the calculations. We suggest that it is perhaps premature to attribute discrepancies between theory and experiment to self-energy effects, which most certainly do exist, before some of these other effects are quantified.

Acknowledgments

This work was supported by the United Kingdom Science and Engineering Research Council. We would like to thank Professor J E Inglesfield for useful discussions.

References

[1] Plummer E W and Eberhardt W 1982 *Adv. Chem. Phys.* **49** 533
[2] Smith N V 1988 *Rep. Prog. Phys.* **51** 1227
[3] Berglund C N and Spicer D E 1964 *Phys. Rev.* **136** A1030
[4] Dose V 1985 *Surf. Sci. Rep.* **5** 337
[5] Kane E O 1964 *Phys. Rev. Lett.* **12** 97

[6] Himpsel F J 1980 *Appl. Opt.* **19** 3964
[7] Willis R F and Feuerbacher B 1978 *Photoemission and the Electronic Properties of Surfaces* ed B Feuerbacher, B Fitton and R F Willis (New York: Wiley) p 281
[8] Goldmann A, Donath M, Altmann W and Dose V 1985 *Phys. Rev.* B **32** 837
[9] Christensen N E and Feuerbacher B 1974 *Phys. Rev.* B **10** 2349
[10] Pendry J B 1976 *Surf. Sci.* **57** 679
[11] Pendry J B 1980 *Phys. Rev. Lett.* **45** 1356
Pendry J B 1981 *J. Phys. C: Solid State Phys.* **14** 1381
[12] Hopkinson J F L, Pendry J B and Titterington D J 1980 *Comput. Phys. Commun.* **19** 69
[13] Thörner G and Borstel G 1984 *Solid State Commun.* **49** 997
[14] Borstel G and Thörner G 1987 *Surf. Sci. Rep.* **8** 1
[15] Nolting W, Braun J, Borstel G and Borgiel W 1990 *Phys. Scr.* **41** 601
[16] Jordan R G and Hoyland M A 1989 *Solid State Commun.* **72** 433
[17] Jordan R G 1989 *J. Phys.: Condens. Matter* **1** 9795
[18] Gollisch H and Feder R 1990 *Solid State Commun.* **76** 237
[19] König U, Weinberger P, Redinger J, Erschbaumer H and Freeman A J 1989 *Phys. Rev.* B **39** 7492
[20] Sobczak E, Nilsson P O and Kanski J 1988 *Phys. Rev.* B **37** 8150
[21] Ackermann B and Feder R 1985 *J. Phys. C: Solid State Phys.* **18** 1093
[22] Braun J, Thörner G and Borstel G 1985 *Phys. Status Solidi* b **130** 643
[23] Ginatempo B, Durham P J, Gyorffy B L and Temmerman W M 1985 *Phys. Rev. Lett.* **54** 1581
[24] Ginatempo B, Durham P J and Gyorffy B L 1989 *J. Phys.: Condens. Matter* **1** 6483
[25] Felter T E, Barker R A and Estrup P J 1977 *Phys. Rev. Lett.* **38** 1138
[26] Debe M K and King D A 1977 *Phys. Rev. Lett.* **39** 708; 1977 *J. Phys. C: Solid State Phys.* **10** L303
[27] King D A and Thomas G 1980 *Surf. Sci.* **92** 201
[28] Inglesfield J E 1985 *Prog. Surf. Sci.* **20** 105
[29] Laine A D 1986 *PhD Thesis* University of Liverpool, unpublished
[30] Collins I R, Law A R and Andrews P T 1988 *J. Phys. C: Solid State Phys.* **21** L655
[31] Riffe D M, Wertheim G K and Citrin P H 1989 *Phys. Rev. Lett.* **63** 1976
[32] Willis R F and Christensen N E 1978 *Phys. Rev.* B **18** 5140
[33] Christensen N E and Willis R F 1979 *J. Phys. C: Solid State Phys.* **12** 167
[34] Schäfer J, Schoppe R, Hölzl J and Feder R 1981 *Surf. Sci.* **107** 290
[35] Drube W, Straub D, Himpsel F J, Soukiassian, P, Fu C L and Freeman A J 1986 *Phys. Rev.* B **34** 8989
[36] Collins I R, Laine A D and Andrews P T *Phys. Rev.* B submitted
[37] Mahan G D 1970 *Phys. Rev.* B **2** 4334
[38] Feibelman P J and Eastman D E 1974 *Phys. Rev.* B **10** 4932
[39] Temmerman W M and Begley A M 1990 private communication
[40] Billington R L and Rhodin T N 1978 *Phys. Rev. Lett.* **41** 1602
[41] Tarng M L and Wehner G K 1973 *J. Appl. Phys.* **44** 1534
[42] K-Rohkonen O and Krause M O 1974 *At. Data Nucl. Data Tables* **14** 139
[43] Swanson L W and Crouser L C 1966 *Phys. Rev. Lett.* **16** 389
[44] Smith K E, Elliott G S and Kevan S D 1990 *Phys. Rev.* B **42** 5385
[45] Hermanson J 1977 *Solid State Commun.* **22** 9
[46] Borstel G, Neumann M and Wöhlecke M 1981 *Phys. Rev.* B **23** 3121
[47] Hohenberg P and Kohn W 1964 *Phys. Rev.* **136** 864
Kohn W and Sham L J 1965 *Phys. Rev.* **140** A1133
[48] Speier W, Zeller R and Fuggle J C 1985 *Phys. Rev.* B **32** 3597
[49] Citrin P H and Wertheim G K 1983 *Phys. Rev.* B **27** 3176
[50] Spanjaard D, Guillot C, Desjonquères M C, Tréglia G and Lecante J 1985 *Surf. Sci. Rep.* **5** 1
[51] Purcell K G 1988 *PhD Thesis* University of Liverpool, unpublished
[52] Wertheim G K, Citrin P H and van der Veen J F 1984 *Phys. Rev.* B **30** 4343
[53] McRae E G 1976 *Surf. Sci.* **57** 761
[54] Dhar S and Kevan S D 1990 *Phys. Rev.* B **41** 8516
[55] Dose V and Reusing G 1980 *Appl. Phys.* **23** 131
[56] Feibelman P J 1975 *Phys. Rev.* B **12** 1319